Kinetic Characteristics of Electrochemical Reduction of SiO Granules in Molten CaCl

AUTHOR(S):

Yang, Xiao; Yasuda, Kouji; Nohira, Toshiyuki; Hagiwara, Rika; Homma, Takayuki

CITATION:

Yang, Xiao ...[et al]. Kinetic Characteristics of Electrochemical Reduction of SiO Granules in Molten CaCl. Journal of The Electrochemical Society 2014, 161(7): D3116-D3119

ISSUE DATE:

2014-05-22

URL:

http://hdl.handle.net/2433/250840

Kinetic Characteristics of Electrochemical Reduction of SiO_2 Granules in Molten $CaCl_2$

Xiao Yang[a,*], Kouji Yasuda[a,b], Toshiyuki Nohira[a,*,z], Rika Hagiwara[a,*], and Takayuki Homma[c,*]

[a] Graduate School of Energy Science, Kyoto University, Yoshida-honmachi, Sakyo-ku, Kyoto 606-8501, Japan

[b] Environment, Safety and Health Organization, Kyoto University, Yoshida-honmachi, Sakyo-ku, Kyoto 606-8501, Japan

[c] Faculty of Science and Engineering, Waseda University, 3-4-1 Okubo, Shinjuku-ku, Tokyo 169-8555, Japan

* Electrochemistry Society Active Member

[z] E-mail: nohira@energy.kyoto-u.ac.jp

Abstract

The kinetic characteristics of electrochemical reduction of SiO_2 granules in molten $CaCl_2$ were investigated to develop a new process for producing solar-grade silicon. The reduction rate was evaluated based on the time dependence of the reduction fractions measured from the growth of the reduced Si layer and the weight change of the samples during electrolysis. The samples were prepared by potentiostatic electrolysis of SiO_2 granules in molten $CaCl_2$ at 1123 K. The results indicated that the reduction was fast at the initial stage of electrolysis, and gradually slowed as the reaction progressed. The apparent current density reached 0.7 A cm^{-2} at the initial stage, which was comparable to the commercial Hall-Héroult process for aluminum production.

Key Words: Solar-grade Silicon, Silica, Electrolysis, Molten Salt, Kinetics, Current Density

Introduction

The global solar cell market has grown rapidly over the past decade. The annual installation of solar cells in the world reached 28.6 GW in 2012.[1] Crystalline silicon is the most prevalent raw material for solar cells on the market, and Si-based solar cells accounted for 88% of the global production in 2012.[2] With the expansion of the market, the consumption of solar-grade silicon (SOG-Si; 6N purity) has also climbed dramatically. An average growth of 10–20% per year is estimated for SOG-Si production over the next decade.

The Siemens process,[3-5] based on hydrogen reduction and thermal decomposition of trichlorosilane ($SiHCl_3$), is the most widely used process for SOG-Si production. In spite of the highly reliable product quality, this process has some disadvantages, including low productivity, low reaction efficiency, and high energy consumption. Therefore, a novel, high yielding, inexpensive SOG-Si production process is required.

Various SOG-Si production processes have been developed to displace the Siemens process.[6-25] Meanwhile, the authors[26-33] and other researchers[34-43] have demonstrated that solid silica (SiO_2) can be directly reduced to solid Si via electrolysis in molten salts. A SiO_2 plate or pellet in contact with a current conductor is electrochemically reduced to Si at the three-phase zone of SiO_2/molten salt/conductor. The produced O^{2-} ions are transferred to the carbon anode through the melt, and then oxidized to form CO or CO_2. The authors has proposed a new SOG-Si production process by

combining this method with the use of high-purity silica and directional solidification,[32] and demonstrated that impurities in the produced Si can be controlled at a low level when high-purity SiO_2 is used as the raw material.[44]

Recently, the authors proposed an improved electrochemical process in which SiO_2 granules are directly used as the raw material.[45] From the viewpoint of industrial application in the future, granules have advantages in cost and quality control over plates or pellets, as well as the suitability for a continuous operation. SiO_2 granules are supplied from the top of the electrolysis cell and are stratified on the cathode placed at the bottom of the cell. The electrochemically reduced Si in molten $CaCl_2$ is tapped out from the cell bottom as slurry containing molten $CaCl_2$. The advantage of this process is the compatibility for a semi-continuous operation, which improves the productivity.

The kinetics of the direct electrochemical reduction of solid SiO_2 granules is crucial for the scale up of the laboratory experiment for commercial production. Previously, the kinetics was studied based on the current-time curve during electrolysis[45] and direct observation of the reaction interface.[46] The overall reduction was clarified to proceed via two different routes: (1) from the SiO_2 granules near the conductor to the distant granules along the granule surfaces, and (2) from the surface to the core in each partly reduced granule. Formation of the core (SiO_2)–shell (Si) structure for partly reduced SiO_2 granules indicated that the reduction along the granule surfaces was faster than that from the surface to the core.

In the present study, the kinetic characteristics of the electrochemical reduction of SiO_2 granules in molten $CaCl_2$ at 1123 K were further investigated by the direct measurement of the reaction interfaces and the weight change of the samples during electrolysis. The kinetics was discussed by plotting the time dependence of the reduction fraction. The productivity of the proposed process was evaluated based on the apparent current density calculated from the experimental results.

Experimental

An Al_2O_3 crucible (Nikkato Corp., o.d. 90 × i.d. 80 × height 100 mm) charged with 300 g of $CaCl_2$ (Kojundo Chemical Lab. Co., Ltd., 99%) was set inside a SiO_2 vessel and heated to 1123 K in a dry Ar atmosphere (100 mL min^{-1}) in an electric furnace. Prior to the experiment, $CaCl_2$ was dried under vacuum at 453 K for 72 h and 773 K for 24 h. The working electrode comprised an Al_2O_3 tube (Nikkato Corp. o.d. 13 × i.d. 9 × height 10 mm) and a Si plate (Nilaco Corp., □15.0 × thickness 0.5 mm, n-type, (100) plane, resistivity 0.1–1.0 Ω cm) (Figure 1). A nickel wire (Nilaco Corp., □1.0 mm, 99%) used as the current lead was connected to the Si plate by threading into a drilled hole (□1.1 mm). Approximately 0.41 g of high-purity SiO_2 granules (Taiheiyo Cement Corp., particle size < 0.1 mm) was charged in the Al_2O_3 tube. With this setup, electrical contact to SiO_2 occurs only through the Si plate at the bottom of the Al_2O_3 tube.

Fig. 1

A glassy carbon rod (Tokai Carbon Co., Ltd., □5.2 mm) was used as the counter electrode. The

reference electrode was a Ag^{+}/Ag electrode prepared by immersing a silver wire (Nilaco Corp., □1.0 mm, 99%) in a $CaCl_2$ melt containing 0.5 mol% AgCl (Wako Pure Chemical Co., Ltd., 99.5%) in a mullite tube (Nikkato Corp., o.d. 6 × i.d. 4 × height 450 mm). The potential of this reference electrode was occasionally checked against a Ca^{2+}/Ca dynamic reference electrode, prepared galvanostatically on a Mo wire (Nilaco Corp., □1.0 mm, 99.95%).[31] All potentials are given with reference to the Ca^{2+}/Ca potential.

After immersing the electrodes in the $CaCl_2$ melt, the potential of the working electrode was set at 0.5 V vs. Ca^{2+}/Ca for the potentiostatic electrolysis for 10 min to 240 min. The working electrode was immediately taken out from the melt after electrolysis and a new one was immersed in for another run. The post-electrolysis working electrode was cut vertically into two halves with a diamond wheel saw (SBT 650, Meiwafosis Co., Ltd.) to observe the cross section and measure the thickness of the reduced layer. The kinetics was evaluated by measuring the weight change of the sample between before and after electrolysis. After electrolysis, the sample was first washed in 1M HCl for 24 h. Here, byproducts like $CaSiO_3$, CaO and $CaCO_3$ react with HCl leaving SiO_2 as the only solid residue. Then, the sample was further washed in distilled water for 48 h, and weighed after drying.

Blank electrolysis tests using the working electrodes without charging SiO_2 granules were conducted before and during the experiment. Large and unstable background currents (*ca.* -100 mA)

were detected, which were mainly due to the side electrochemical reactions of moisture. Since the area of Si plate contacting only the molten salt was larger than the area contacting SiO_2 granules (See Fig. 1b), it was difficult to precisely evaluate the current corresponding only to the SiO_2 reduction.

Results and Discussion

Growth of Reduced Layer. —The cross sections of the working electrodes after electrolysis at 0.5 V vs. Ca^{2+}/Ca for (a) 10 min, (b) 30 min, (c) 60 min, and (d) 120 min in molten $CaCl_2$ at 1123 K are shown in Figure 2. For each sample, a dark brown layer was observed above the Si plate at the bottom. Formation of crystalline Si in this layer was confirmed by XRD and SEM/EDX in a previous study with a similar experimental setup.[46]

Fig. 2

The dark layer, composed of reduced Si, grows from the bottom to the top with the progress of electrolysis. After 120 min of electrolysis, most of the colorless 6.0-mm-thick SiO_2 layer became dark. The top position of unreduced SiO_2 layer did not apparently change after reduction, as seen in Figure 2. This indicates that the granules piled on the Si plate as a whole do not shrink downward during the reduction. In the similar manner as quartz plate,[26] the volume decrease from SiO_2 to Si is explained by the formation of porous structure inside the granule. The thicknesses of the dark layer at three different positions for each image in Figure 2 were measured using a ruler. The average

Fig. 3

value of the reduced layer is plotted against electrolysis time in Figure 3. The growth rate of the reduced layer gradually decreased with the electrolysis progress.

Weight Change during Electrolysis.— The progress of the electrochemical reduction was investigated by measuring the weight change of the samples. The mass balance before and after electrolysis is illustrated in Figure 4, where $W_{bef.}$ and $W_{aft.}$ are the weights of the samples before and after electrolysis. Here, the dissolution of solid SiO_2 in molten $CaCl_2$ is not considered. Because the Si atoms remain in the tube during the electrolysis, the weight change occurs by the removal of oxygen. The weight change after 10–240 min of electrolysis are listed in Table I and plotted against electrolysis time in Figure 5. In accordance with the growth rate of the reduced layer, the rate of the weight change is large at the initial stage of electrolysis compared with the later stage.

Fig. 4

Table I

Fig. 5

Reduction Fraction during Electrolysis.— The reduction fraction was evaluated by two methods. From the perspective of the growth of the reduced layer, the apparent reduction fraction ($F_{app.}$) is defined as

$$F_{app.} = \frac{\delta_{red.}}{\delta_{ini.}} \times 100\% \quad (1)$$

where $\delta_{red.}$ and $\delta_{ini.}$ are the thicknesses of the reduced layer and the initial SiO_2 layer (Figure 2). Secondly, the actual reduction fraction ($F_{act.}$) is calculated from the weight change of the samples

137 during electrolysis by

$$F_{\text{act.}} = \frac{(W_{\text{bef.}} - W_{\text{aft.}}) \cdot \dfrac{M_{\text{SiO}_2}}{2M_{\text{O}}}}{W_{\text{bef.}}} \times 100\% \quad (2)$$

139 where M_{SiO2} and M_O are the molar weights of SiO_2 and O, respectively.

140 The apparent and actual reduction fractions are listed in Table II. The time dependences of the Table II

141 reduction fractions are compared in Figure 6. The apparent reduction fraction was larger than the Fig. 6

142 actual value. The difference is due to the formation of the core (SiO_2)–shell (Si) structure for the

143 partly reduced SiO_2 granules (Figure 7).[46] The SiO_2 granules in the reduced layer were not Fig. 7

144 completely reduced to Si.

145 $F_{app.}$ and $F_{act.}$ rapidly increased at the initial stage of electrolysis as compared with the later stage.

146 This tendency indicates that the reduction gradually slows with the progress of electrolysis, and two

147 potential explanations can be considered. First, contact resistance exists between formed Si particles,

148 resulting in a voltage drop. With the progress of electrolysis, the reduction front gradually moves

149 away from the start point (Si plate) leading to a large voltage loss by contact resistance. The

150 reduction rate has been reported to decrease at more positive potentials.[26,27,29] Because the contact

151 resistance would be primarily generated at the surface of Si granules, this effect plays an important

152 role on the behavior of $F_{app.}$. Moreover, the diffusion of O^{2-} ions in $CaCl_2$ inside the granules

153 becomes important when the reduction proceeds. For the reduction along the granule surface, the

154 formed O^{2-} ions immediately diffuse into the bulk $CaCl_2$. For the reduction inside, the formed O^{2-}

ions must diffuse through the crevice of the Si shell. As explained in the previous study,[45,46] the O^{2-} ions accumulate in the $CaCl_2$ in the crevice, leading to an increased viscosity of $CaCl_2$ and decreased diffusion coefficient of the O^{2-} ions. Consequently, the reduction rate decelerates with the progress of electrolysis, which is predominantly responsible for the behavior of $F_{act.}$.

Apparent Current Density.— The current density, an important kinetic index, is evaluated from the weight change of the samples. The electrochemical reduction of SiO_2 is written as

$$SiO_2\ (s) + 4e^- \rightarrow Si\ (s) + 2O^{2-} \tag{3}$$

The quantity of cathodic electric charge (Q) used for the reduction of SiO_2 can be calculated by

$$Q = \frac{W_{\mathbf{bef.}} - W_{\mathbf{aft.}}}{2M_{\mathbf{O}}} \times 4e \cdot N_{\mathbf{A}} \tag{4}$$

where e is the elementary charge of an electron ($e \approx 1.6\times10^{-19}$ C), and N_A is Avogadro's constant ($N_A \approx 6.02\times10^{23}$ mol^{-1}). The apparent current density (J) based on the geometric area of the bottom conductor (Si plate in Figure 1) can be obtained by

$$J = \frac{Q}{A \cdot t} = \frac{Q}{\pi \cdot \frac{d^2}{4} \cdot t} \tag{5}$$

where A is the valid geometrical area of the Si plate, d is the inner diameter of the Al_2O_3 tube (d = 0.9 cm), and t is the electrolysis time. In the present study, cathodic charge and current are taken as positive values.

The calculated apparent current density is listed in Table II, and its time dependence is shown in

Fig. 8

Figure 8. The current density was as large as 0.7 A cm^{-2} at the initial stage, ca. 20 min, and gradually decreased with the progress of electrolysis. This value is comparable to the current density of the commercial Hall-Héroult process for aluminum production.[47] This result indicates that the direct electrochemical reduction of SiO_2 in molten $CaCl_2$ has the potential of being a highly productive silicon production process.

Conclusions

The kinetic characteristics of the electrochemical reduction of SiO_2 granules in molten $CaCl_2$ at 1123 K were investigated by direct observation of cross-sectioned samples and weight change of samples during electrolysis.. The results indicated that the reduction was fast at the initial stage of electrolysis and gradually slowed as the electrolysis progressed. The apparent current density reached 0.7 A cm^{-2} at the initial stage of electrolysis. The direct electrochemical reduction of SiO_2 in molten $CaCl_2$ has the potential of being a silicon production process with high productivity comparable to the commercial Hall-Héroult process.

Acknowledgements

189 This study was partly supported by JST-CREST and Grants-in-Aid for Scientific Research A from
190 the Japan Society for the Promotion of Science (JSPS). We thank Taiheiyo Cement Corporation for
191 providing high purity SiO_2 granules.

192

References

1. *Global market outlook for photovoltaics 2013-2017*, European Photovoltaic Industry Association, Brussels (2013).
2. *Rare Metal News*, Arumu Publishing Co., Tokyo (2013).
3. H. Schweickert, K. Reuschel, and H. Gutsche, U.S. patent 3,011,877 (1961).
4. H. Gutsche, U.S. patent 3,042,494 (1962).
5. H. Oda, *Kogyo Zairyo*, **55**, 30 (2007).
6. H. S. N. Setty, C. L. Yaws, B. R. Martin and D. J. Wangler, U.S. Patent 3,963,838 (1976).
7. S. Wakamatsu and H. Oda, PCT International Patent, WO2001/085613 (2001).
8. W. Dieter, European Patent 1,544,167 (2005).
9. K. Yasuda, K. Morita, T. H. Okabe, *Energy Technology*, **2**, 141 (2014).
10. S. Honda, M. Yasueda, S. Hayashida and M. Yamaguchi, Japanese Patent Application, H19-145663 (2007).
11. K. Saegusa and T. Yamabayashi, PCT International patent WO2007/001093 (2007).
12. K. Yasuda and T. H. Okabe, *JOM*, **62**, 94 (2010).
13. K. Yasuda, K. Saegusa, and T. H. Okabe, *Metall. Mater. Trans. B*, **42**, 37 (2011).
14. K. Suzuki, T. Kumagai and N. Sano, *ISIJ Int.*, **32**, 630 (1992).
15. T. Ikeda and M. Maeda, *ISIJ Int.*, **32**, 635 (1992).

16. N. Yuge, H. Baba and F. Aratani, U.S. Patent 5,182,091 (1993) .

17. Y. Sakaguchi, M. Ishizaki, T. Kawahara, M. Fukai, M. Yoshiyagawa and F. Aratani, *ISIJ Int.*, **32**, 643 (1992).

18. M. D. Johnston, L. T. Khajavi, M. Li, S. Sokhanvaran and M. Barati, *JOM*, **64**, 935 (2012).

19. T. Yoshikawa and K. Morita, *JOM*, **64**, 946 (2012).

20. J. Sanchez, J. Barona, E. Conejero, M. Canle, X. Rel, P. Garcia, and M. Martinez, U.S. Patent US008168123B2 (2012).

21. B. G. Gribov and K. V. Zinov'ev, *Inorg. Mater.*, **39**, 653 (2003).

22. D. Elwell and R. S. Feigelson, *Sol. Energy Mater.*, **6**, 123 (1982).

23. D. Elwell and G. M. Rao, *J. Appl. Electrochem.*, **18**, 15 (1988).

24. J. Olson and K. Carleton, *J. Electrochem. Soc.*, **128**, 2698 (1981).

25. J. Cai, X. Luo, G. M. Haarberg, O. E. Kongstein, and S. Wang, *J. Electrochem. Soc.*, **159**, D155 (2012).

26. T. Nohira, K. Yasuda, and Y. Ito, *Nat. Mater.*, **2**, 397 (2003).

27. K. Yasuda, T. Nohira, K. Amezawa, Y. H. Ogata, and Y. Ito, *J. Electrochem. Soc.*, **152**, D69 (2005).

28. K. Yasuda, T. Nohira, Y. H. Ogata, and Y. Ito, *Electrochim. Acta*, **51**, 561 (2005).

29. K. Yasuda, T. Nohira, and Y. Ito, *J. Phys. Chem. Solids*, **66**, 443 (2005).

30. K. Yasuda, T. Nohira, Y. H. Ogata, and Y. Ito, *J. Electrochem. Soc.*, **152**, D208 (2005).

31. K. Yasuda, T. Nohira, R. Hagiwara, and Y. H. Ogata, *J. Electrochem. Soc.*, **154**, E95 (2007).

32. K. Yasuda, T. Nohira, R. Hagiwara, and Y. H. Ogata, *Electrochim. Acta*,. **53**, 106 (2007).

33. K. Yasuda, T. Nohira, K. Takahashi, R. Hagiwara, and Y. H. Ogata, *J. Electrochem. Soc.*, **152**, D232 (2005).

34. W. Xiao, X. Wang, H. Yin, H. Zhu, X. Mao, and D. Wang, *RSC Advances,* **2**, 7588 (2012).

35. X. Jin, P. Gao, D. Wang, X. Hu, and G. Z. Chen, *Angew. Chem.*, **116**, 751 (2004).

36. P. C. Pistorius and D. J. Fray, *J. S. Afr. Inst. Min. Metall.*, **106**, 31 (2006).

37. W. Xiao, X. Jin, Y. Deng, D. Wang, X. Hu, and G. Z. Chen, *ChemPhysChem.,* **7**, 1750 (2006).

38. W. Xiao, X. Jin, Y. Deng, D. Wang, X. Hu, and G. Z. Chen, *J. Electroanal. Chem.*, **639**, 130 (2010).

39. S. K. Cho, F. F. Fan, and A. J. Bard, *Electrochim. Acta*, **65**, 57 (2012).

40. E. Juzeliunas, A. Cox, and D. J. Fray, *Electrochem. Comm.*, **12**, 1270 (2010).

41. E. Ergül, İ. Karakaya, and M. Erdoğan, *J. Alloy. Compd*., **509**, 89 (2011).

42. Y. Jiang, J. Xu, X. Guan, U.B. Pal, and S.N. Basu, *MRS Proceedings*, **1493**, 231(2013).

43. T. Oishi, M. Watanabe, K. Koyama, M. Tanaka, and K. Saegusa, *J. Electrochem. Soc.*, **158**, E93(2011).

44. K. Yasuda, T. Nohira, K. Kobayashi, N. Kani, T. Tsuda, and R. Hagiwara, *Energy Technology*, **1**,

245 (2013).

45. T. Toba, K. Yasuda, T. Nohira, X. Yang, R. Hagiwara, K. Ichitsubo, K. Masuda, and T. Homma, *Electrochem.*, **81**, 559 (2013).

46. X. Yang, K. Yasuda, T. Nohira, R. Hagiwara, and T. Homma, *Metall. Mater. Trans. B*, in press (2014). doi:10.1007/s11663-014-0056-5

47. J. W. Evans, *JOM*, **59**, 30 (2007).

253 **Caption List**

254 Table I. Weight change of samples during electrolysis at 0.5 V vs. Ca^{2+}/Ca for 10-240 min in molten
255 $CaCl_2$ at 1123 K.

256 Table II. Apparent reduction fraction ($F_{app.}$), actual reduction fraction ($F_{act.}$), and apparent current
257 density of direct electrochemical reduction of SiO_2 granules by electrolysis at 0.5 V vs.
258 Ca^{2+}/Ca for 10-240 min in molten $CaCl_2$ at 1123 K.

259

260 Figure 1. (a) Schematic illustration and (b) photograph of the working electrode.

261 Figure 2. Photographs of the cross sections of working electrodes after electrolysis at 0.5 V vs.
262 Ca^{2+}/Ca for 10-120 min in molten $CaCl_2$ at 1123 K.

263 Figure 3. Time dependence of the thickness of the reduced layer of electrochemical reduction of
264 SiO_2 granules by electrolysis at 0.5 V vs. Ca^{2+}/Ca for 10-120 min in molten $CaCl_2$ at 1123 K.

265 Figure 4. Schematic illustration of mass balance during electrolysis.

266 Figure 5. Time dependence of weight change of samples during electrolysis at 0.5 V vs. Ca^{2+}/Ca for
267 10-240 min in molten $CaCl_2$ at 1123 K.

268 Figure 6. Time dependences of reduction fractions of electrochemical reduction of SiO_2 granules by
269 electrolysis at 0.5 V vs. Ca^{2+}/Ca for 10-240 min in molten $CaCl_2$ at 1123 K.

270 Figure 7. Schematic illustrations of the (a) cross section of the working electrode half way through
271 electrolysis and (b) core (SiO_2)-shell (Si) structure for partly reduced SiO_2 granules.

272 Figure 8. Time dependence of the apparent current density of electrochemical reduction of SiO_2
273 granules by electrolysis at 0.5 V vs. Ca^{2+}/Ca for 10-240 min in molten $CaCl_2$ at 1123 K.

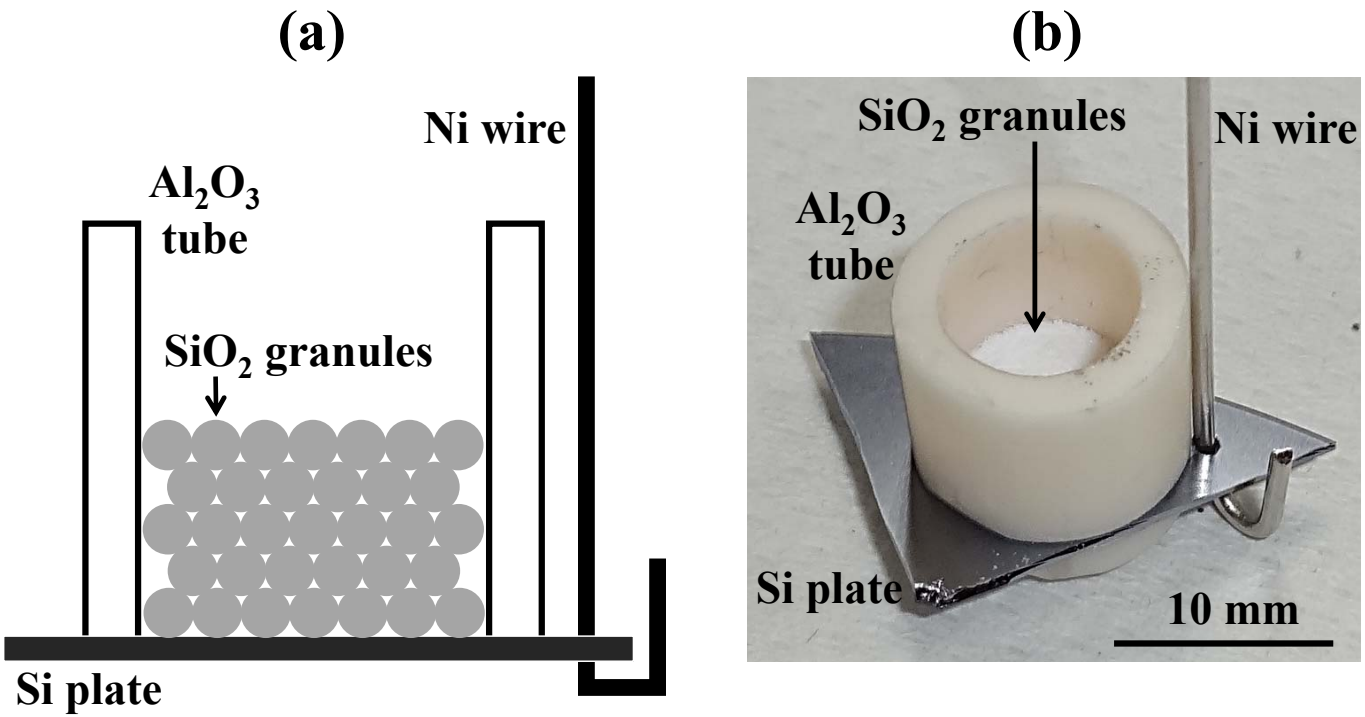

Figure 1. (a) Schematic illustration and (b) photograph of the working electrode.

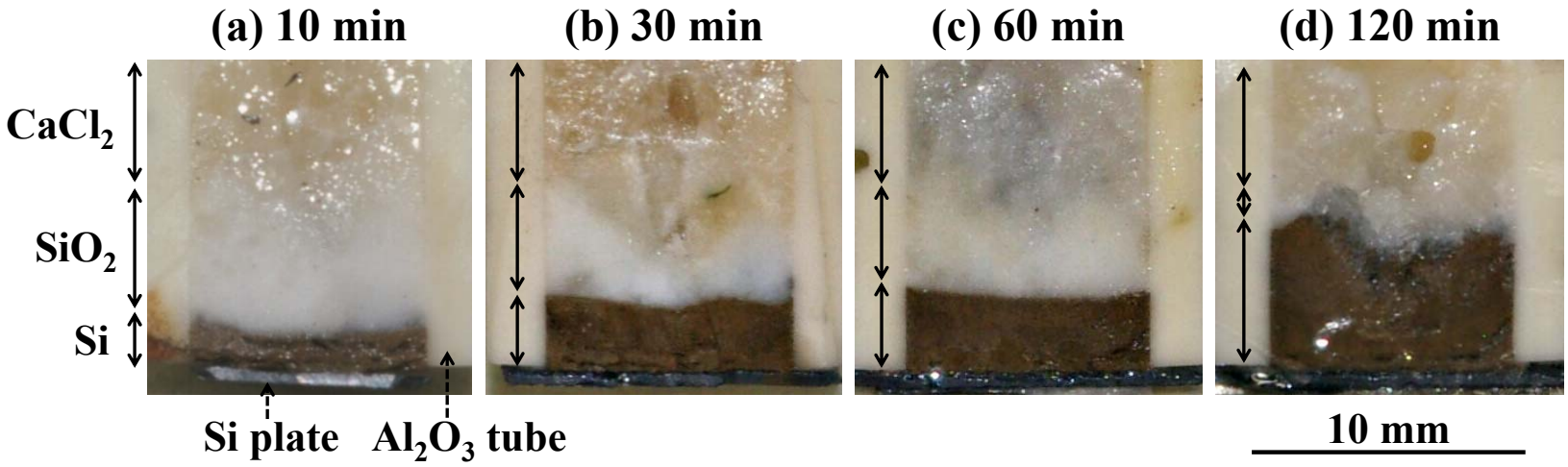

Figure 2. Photographs of the cross sections of working electrodes after electrolysis at 0.5 V vs. Ca^{2+}/Ca for 10-120 min in molten $CaCl_2$ at 1123 K.

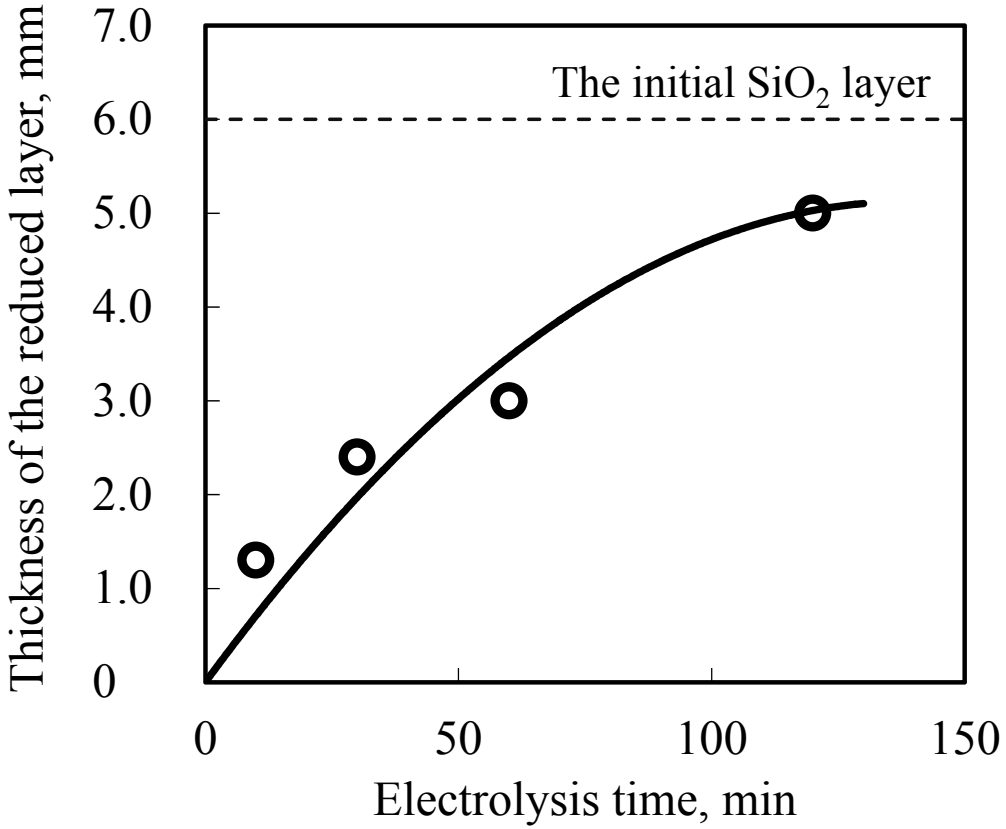

Figure 3. Time dependence of the thickness of the reduced layer of electrochemical reduction of SiO_2 granules by electrolysis at 0.5 V vs. Ca^{2+}/Ca for 10-120 min in molten $CaCl_2$ at 1123 K.

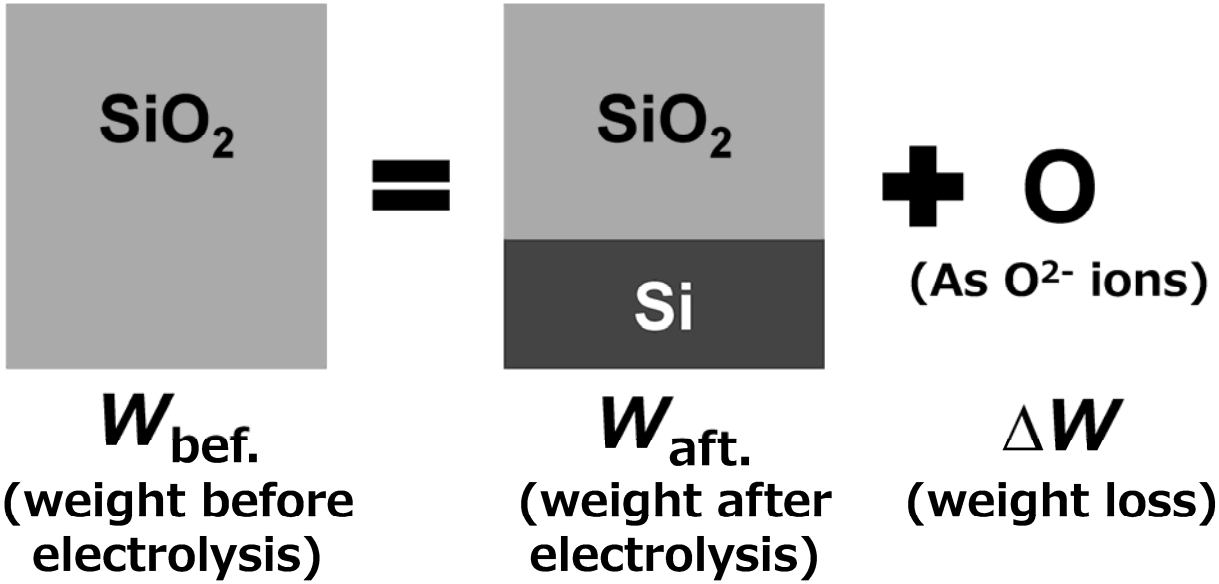

Figure 4. Schematic illustration of mass balance during electrolysis.

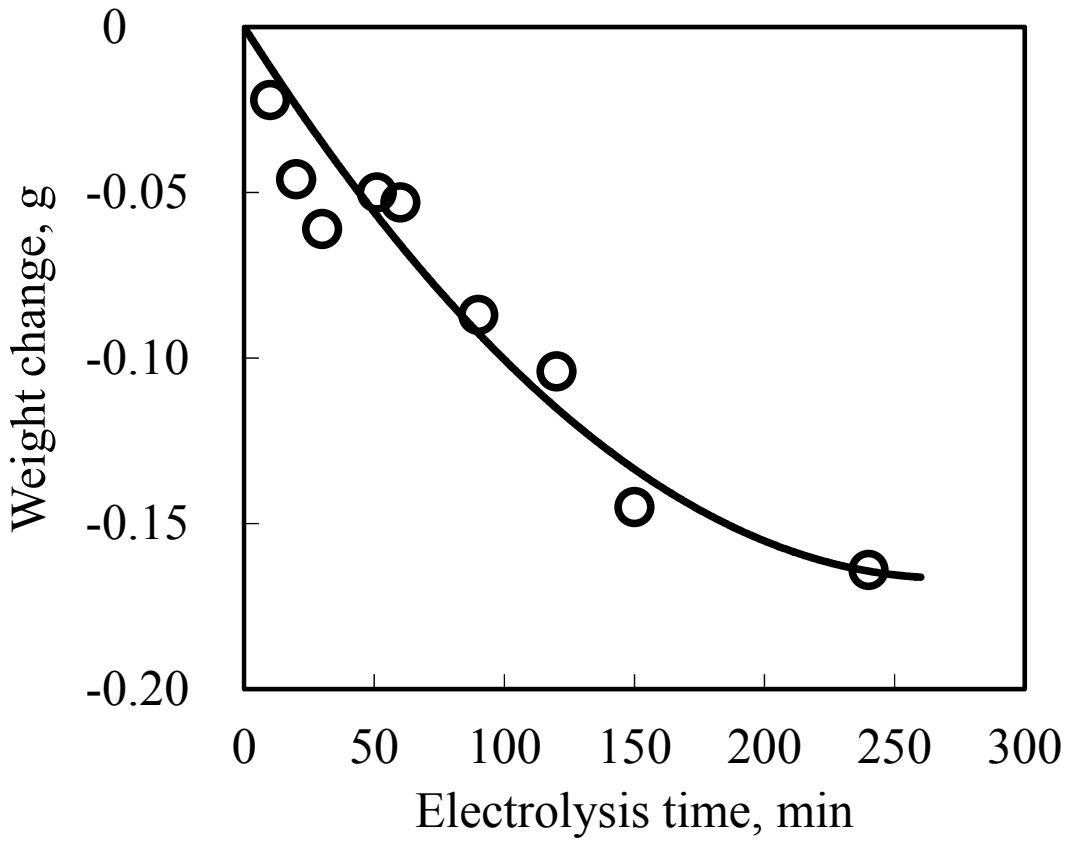

Figure 5. Time dependence of weight change of samples during electrolysis at 0.5 V vs. Ca^{2+}/Ca for 10-240 min in molten $CaCl_2$ at 1123 K.

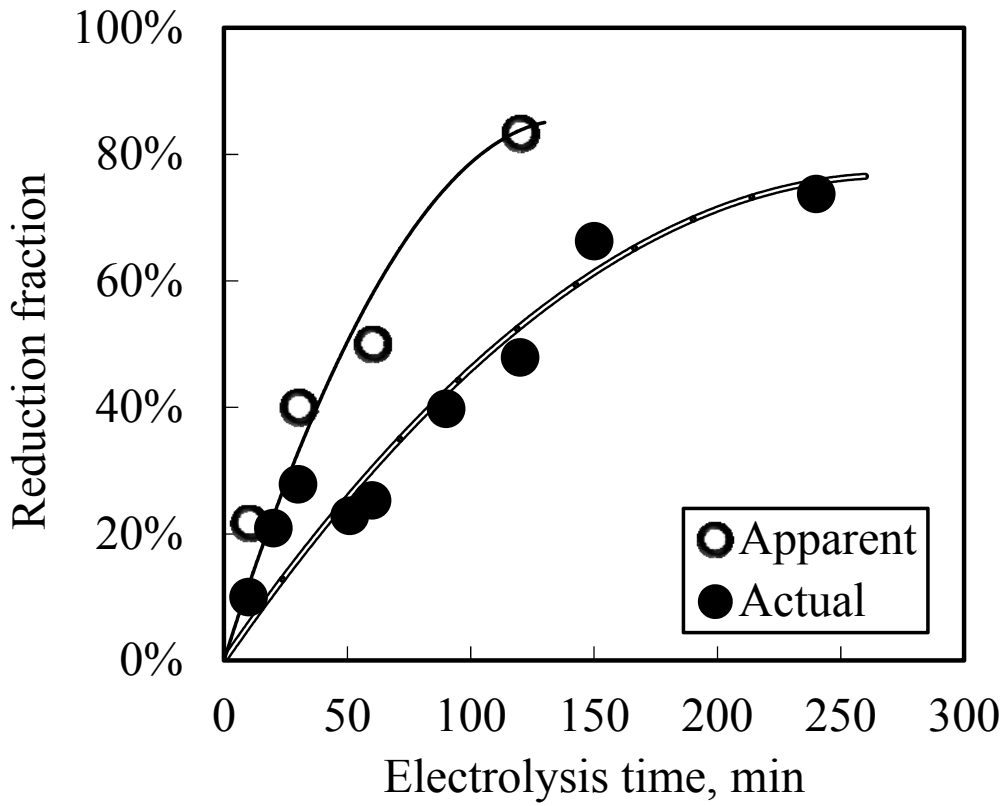

Figure 6. Time dependences of reduction fractions of electrochemical reduction of SiO_2 granules by electrolysis at 0.5 V vs. Ca^{2+}/Ca for 10-240 min in molten $CaCl_2$ at 1123 K.

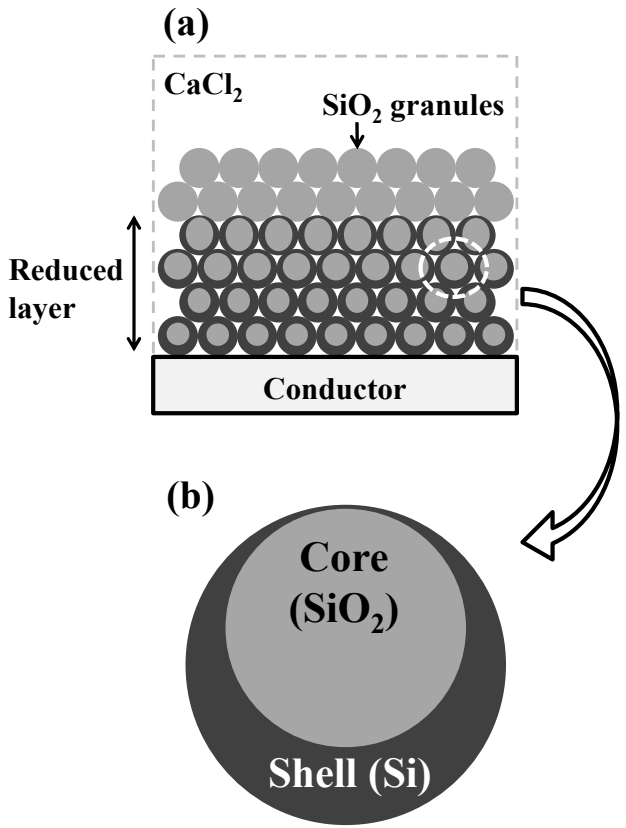

Figure 7. Schematic illustrations of the (a) cross section of the working electrode half way through electrolysis and (b) core (SiO_2)-shell (Si) structure for partly reduced SiO_2 granules.

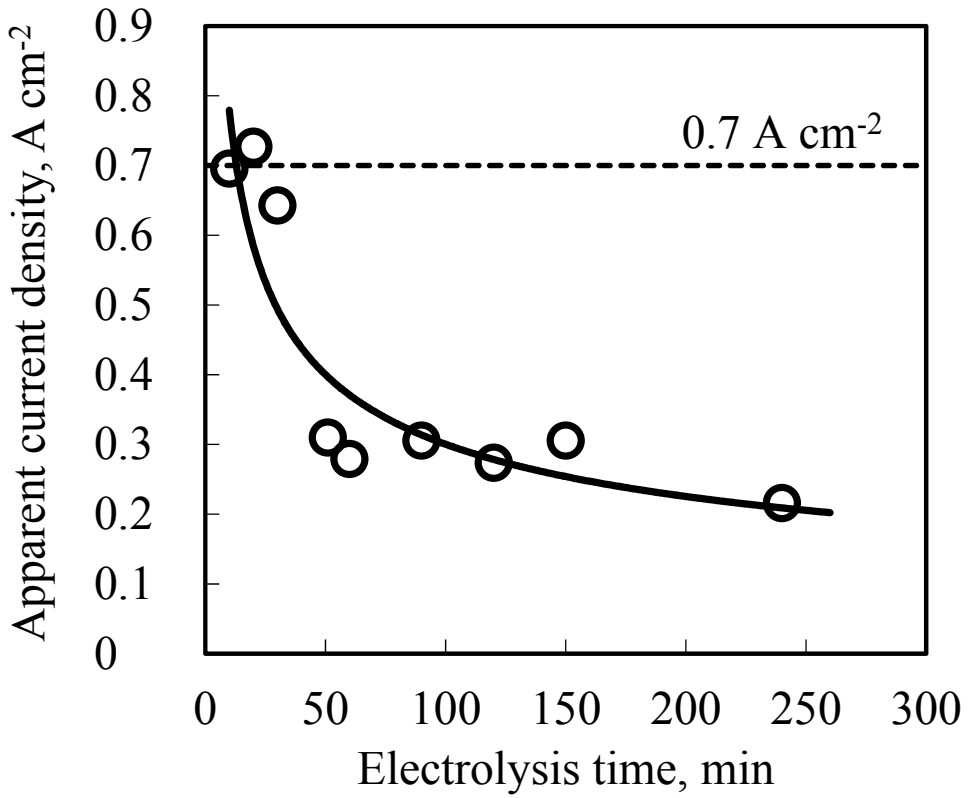

Figure 8. Time dependence of the apparent current density of electrochemical reduction of SiO_2 granules by electrolysis at 0.5 V vs. Ca^{2+}/Ca for 10- 240 min in molten $CaCl_2$ at 1123 K.

Table I. Weight change of samples during electrolysis at 0.5 V vs. Ca^{2+}/Ca for 10-240 min in molten $CaCl_2$ at 1123 K.

Exp. No.	Time /min	Weight of the sample /g		Weight change /g
		Before electrolysis	After electrolysis	
2-1	10	0.413	0.391	-0.022
2-2	20	0.413	0.367	-0.046
2-3	30	0.411	0.350	-0.061
2-4	50	0.410	0.360	-0.050
2-5	60	0.393	0.340	-0.053
2-6	90	0.410	0.323	-0.087
2-7	120	0.407	0.303	-0.104
2-8	150	0.410	0.265	-0.145
2-9	240	0.417	0.253	-0.164

Table II. Apparent reduction fraction ($F_{app.}$), actual reduction fraction ($F_{act.}$), and apparent current density of direct electrochemical reduction of SiO_2 granules by electrolysis at 0.5 V vs. Ca^{2+}/Ca for 10-240 min in molten $CaCl_2$ at 1123 K.

Exp. No.	Time /min	$F_{app.}$	$F_{act.}$	Apparent current density /A cm^{-2}
1-1	10	21.7%	-	-
1-2	30	40.0%	-	-
1-3	60	50.0%	-	-
1-4	120	83.3%	-	-
2-1	10	-	10.0%	0.70
2-2	20	-	20.9%	0.73
2-3	30	-	27.8%	0.64
2-4	50	-	22.9%	0.31
2-5	60	-	25.3%	0.28
2-6	90	-	39.8%	0.31
2-7	120	-	47.9%	0.27
2-8	150	-	66.3%	0.31
2-9	240	-	73.7%	0.22